RSC Advances

ROYAL SOCIETY OF CHEMISTRY

www.rsc.org/advances

Table of Contents Entry

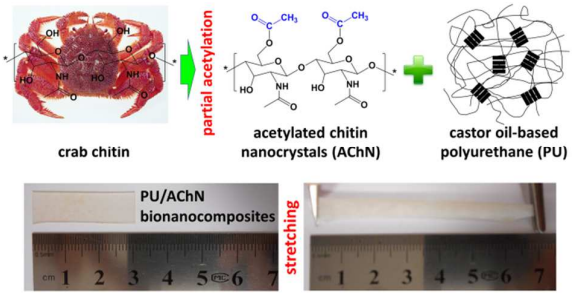

Novel elastomeric nanocomposites from "rigid" partially-acetylated chitin nanocrystals and "soft" high-elasticity polyurethane.

RSC Advances

RSCPublishing

ARTICLE

Green bionanocomposites from high-elasticity "soft" polyurethane and high-crystallinity "rigid" chitin nanocrystals with controlled surface acetylation

Cite this: DOI: 10.1039/xoxxoooooox

Received ooth January 2012,
Accepted ooth January 2012

DOI: 10.1039/xoxxoooooox

www.rsc.org/

Ning Lin,[a,b] Siwen Wei,[c] Tao Xia,[a] Fei Hu,[a] Jin Huang,[a*] and Alain Dufresne[b]

Castor oil-based polyurethane bionanocomposites with improved mechanical properties were prepared by the introduction of crab chitin nanocrystals from partial surface acetylation. Through the controlled acetylation, one part of hydrophilic hydroxyl groups on nanocrystals were replaced by hydrophobic acetyl groups in order to enhance the compatibility between chitin nanoparticles and polyurethane; and other part of hydroxyl groups were preserved on the surface of nanocrystals for the purpose of rigid network formation among chitin nanoparticles. The presence of acetylated chitin nanocrystals at the moderate concentration (6 wt%) will significantly promote the nano-reinforcing effect in composites, and simultaneously improved the strength, stiffness and toughness of thermoplastic polyurethane-based nanocomposites. Meanwhile, derived from the restriction of rigid nanocrystals to soft segments, the glass transition temperatures of nanocomposites surprisingly increased with the higher loading levels of acetylated chitin nanocrystals. More importantly, this study provided a strategy for the discussion of synergy effects and "tradeoff" of adequate dispersion, network formation and interfacial adhesion of rigid nanoparticles in soft polymeric matrices, by means of structure and properties analysis of semi-transparent polyurethane/acetylated chitin nanocrystals composites.

Introduction

Since the first industrial application of polymer nanocomposites based on polyamide and layered silicates (named Nylon-6),[1] the development of nanoengineered polymeric composite attracts great interest, and rapidly triggers the new class of materials alternative to conventional materials over last twenty years. Derived from reinforcement effect of nanofillers, physical properties of composites can be improved at the molecular level without affecting polymer processibility, such as better mechanical performance, thermal stability and barrier properties. Rubber, also called elastomer, is widely used as polymeric matrix for nanocomposites due to its high elasticity and high elongation at break, but low hardness for the limitation of practical application. The challenges of elastomer-based nanocomposites are both requiring optimum nano-reinforcement through well-dispersion nanofillers inducing good adhesion on the matrix/filler interface, and improving the stiffness of elastomer without sacrificing its high extensibility.[2] Although diverse rubber nanocomposites have been discussed by the introduction of numerous potential nanoelements, most studies focus on the use of layered silicates, carbon nanotubes and inorganic nanoparticles (mainly silica).[3]

Recently, considering the pressure of ecological environment and instable cost of petrochemcials, there is an interesting demand for biobased nanofillers from natural resources in polymer industry to produce low-cost and biodegradable materials. Isolated from the second most natural polymer, chitin nanocrystal (with the synonyms of chitin (nano)whisker and nanocrystalline chitin) is the crystalline component extracted from native chitin, such as exoskeleton of arthropods like crabs, shrimp, squid pens, etc.[4] The first investigation on the preparation of chitin nanocrystals in 1959 was achieved by the treatment of chitin microfibrils with hydrochloric acid solution.[5] During acid hydrolysis, disordered and low lateral ordered regions of chitin are preferentially hydrolyzed and dissolved in the acidic solution, whereas water-insoluble, highly crystalline residues that have higher resistance to acid attack remain intact. Indeed, both nanofibers and nanocrystals can be isolated from chitin sources, but only chitin nanocrystals (ChN) occur as highly crystalline and rigid rod-like (or needle-like) nanoparticles, possessing superior mechanical stiffness (at least 150 GPa),[6] which is an ideal candidate as reinforcing bionanofiller for polymer composites. Nanocomposites incorporating ChN as the reinforcing phase have been reported with diverse matrices involving natural polymers (such as natural rubber, chitosan, alginate, hyaluronan, silk fibroin, soy protein isolate and starch) and synthetic polymers (for instance acrylic resin, poly(S-co-BuA), polycaprolactone, poly(vinyl alcohol) and waterborne polyurethane).[7,8]

As the rigid nanoparticles, the presence of chitin nanocrystals in soft polymers will induce the promising enhancement for ensuring composites, which is expected to develop special-mechanical nanocomposites with both high strength and tenacity. The attempts of reinforcing soft elastomer with pristine ChN have been reported previously on natural rubber[9,10] and water polyurethane.[11-13] However, direct incorporation of pristine ChN with hydrophobic polymers may cause the weak interfacial interaction due to the high hydrophilicity and serious self-aggregation of ChN in apolar

matrices. Therefore, one study proposed chemical modification to tailor the surface properties of ChN, and improve the compatibility of nanoparticles and natural rubber in composites. However, the treatments with phenyl isocyanate, alkenyl succinic anhydride, or 3-isopropenyl-α,α′-dimethylbenzyl isocyanate to the surface of ChN would limit the hydrogen bonding interactions between nanoparticles after these modifications and reduce the driving force of network formation, which caused the poor reinforcing effect and ultimately loss of mechanical properties.[14]

Surface acetylation is generally considered to be a simple, popular and inexpensive approach in chemical modification to change the surface polarity of chitin.[15] In our previous studies, surface acetylation have been performed on cellulose nanocrystals (CNC),[16,17] and proved to be able to control the acetylation degrees with the regulation of acetylated agent ratios and reaction conditions. Partial surface acetylation was performed on ChN for the purpose of both improvement of dispersion and interfacial adhesion between nanocrystals and polymers (filler/matrix), as well as preservation of interactions among nanoparticles for the formation of rigid network. This controlled surface acetylation was achieved by the reaction between acetic anhydride and chitin nanocrystals, which partially converted the hydrophilic hydroxyl groups (–OH) to hydrophobic acetyl groups (–$COCH_3$). On the other hand, castor oil-based polyurethane (PU) elastomer was chosen as the polymeric matrix reinforced by acetylated chitin nanocrystals, which was composed of castor oil as soft segments and a diisocyanate as hard segments. Castor oil is a low-cost, abundantly available, renewable natural resource, and has attracted intensive research resulting from its wide applications in coatings, adhesives, paints, sealants, encapsulating compounds etc.[18,19] Recently, as a polyester macroglycol with reactive hydroxyl functional groups, castor oil has been reported as superior raw materials to prepare bio-based elastomeric polyurethane or waterborne polyurethane materials.[20-24]

The main objective of this study is the properties, interface investigation and enhancing effects discussion of acetylated chitin nanocrystals (rigid nanoparticles) in thermoplastic polyurethane (soft polymer). It is expected that possible interactions between additional carbonyl groups from acetylated chitin nanocrystals and ester groups from castor oil will facilitate the compatibility of nanoparticles and polyurethane. Meanwhile, partially acetylation on chitin nanocrystals ensured the preservation of some hydroxyl groups for the formation of rigid network through hydrogen bonding among nanoparticles. Results of four aspects are included in this work, which are proofs and properties of acetylated chitin nanocrystals, appearance and light transmittance ratio of composites, mechanical and thermal properties of composites, and crystalline property and microstructure of composites. Degree of acetylated substitution (*DS*) on chitin nanocrystals was calculated from the results of elemental analysis, and effect of surface modification to morphology and dimension of nanocrystals was observed by transmission electron microscopy. Atomic force microscopy was used to investigate the surface appearance of composites, and results from UV-spectroscopy proved the semi-transparent nanomaterials of prepared composites. Fourier transform infrared spectroscopy was performed to investigate the presence of modified chitin nanocrystals to microstructure of composites, together with the observation of inner morphology with scanning electronic microscopy. The mechanical performances and thermal properties of nanocomposites were further studied, involving the discussion of reinforcing mechanism and formation of percolating network.

Experimental Section

Materials. Castor oil with a hydroxyl value of 163 mg –OH/g oil was purchased from Shanghai Sinopharm Chemical Reagent Ltd. (Shanghai, China) and vacuum dried at 110 °C for 2 h before use. Native chitin from crab shell was purchased from Yuhuan Ocean Biochemical Ltd. (Zhejiang, China). Acetic anhydride and pyridine was purchased from Xilong Chemical Industry Ltd. (Shantou, China), and dried and purified according to standard procedures. 2,4-toluene diisocyanate (TDI ≥98 %) was purchased from Wuhan Jiangbei Chemical Reagent Ltd. (Hubei, China). 1,4-butanediol, sulfuric acid, tetrahydrofuran (THF) and other analytical grade reagents were used without further purification.

Extraction of Chitin Nanocrystals (ChN). Chitin nanocrystals were extracted from crab shell chitin following previous report.[25] Briefly, crab chitin was boiled and mechanically stirred in the 5 wt% KOH solution to remove the most of proteins, and then bleached with $NaClO_2$ solution for 6 h at 80 °C. Bleached suspension was kept in another 5 wt% KOH solution for 48 h to remove residual proteins. Purified chitin was hydrolyzed with boiling 3 N HCl for 90 min under mechanical stirring, and followed the treatments of washing, centrifugation and dialysis with distilled water. Chitin nanocrystals in white powder were released from freeze-drying.

Acetylation of Chitin Nanocrystals (AChN). Surface acetylation of chitin nanocrystals was performed with constant stirring under a nitrogen atmosphere in a three-necked round-bottomed flask equipped with a condenser. The suspension of chitin nanocrystals (1.0 g) and anhydrous pyridine (20 mL) was dispersed with ultrasonic treatment for 15 min. Chemical reaction between acetic anhydride (AA) and chitin nanocrystals was started by the addition of 5 mL AA in anhydrous pyridine solution to ChN dispersed suspension. The reaction mixture was kept at 80 °C and stirred at 400 rpm (rounds per minute) for 5 h. After the reaction, acetylated ChN was isolated by the precipitation of suspensions in 1.0 L distilled water, and purified by washing with a solution of acetone/water to eliminate all non-bonded chemicals (i.e., unreacted compounds and reaction by-products). The powder of acetylated chitin nanocrystals were released from freeze-drying, and coded as AChN. The chemical reaction of surface acetylation on chitin nanocrystals was shown in Figure 1(A).

Synthesis of Castor Oil-Based Polyurethane (PU) Prepolymer. Castor oil-based polyurethane prepolymer was prepared following the method reported by Gao and Zhang with a litter modification.26 Castor oil was dropped into the flask with desired toluene diisocyanate under a nitrogen atmosphere. The dropping was completed within 30 min, and then the stirring was maintained for 2 h to obtain the PU prepolymer. It should be noted that during the synthesis of PU prepolymer, the value of [NCO]/[OH] in the system was controlled as 2. Chemical structure of NCO terminated PU prepolymer was shown in Figure 1(B).

Preparation of PU/AChN Nanocomposites. PU prepolymer (5 g) was mixed with the desired mass of AChN and 1,4-butanediol as the chain extender in tetrahydrofuran (THF) at room temperature. The value of [NCO]/[OH] in the system was regulated as 1 via the addition of 1,4-butanediol. Figure 1(C) showed the chain extension reaction between prepolymer and butanediol, together with the synthesis of castor oil-based PU material. The resulting mixture with solid content (nonvolatile components) was given about 30 wt% by adding THF, and casted on the polytetrafluoroethene mold. The mixture was cured at room temperature for two days to evenly evaporate the solvent, and formed the dried films with the thickness of about 0.5 mm. The prepared PU/AChN nanocomposites containing different AChN contents (2, 4, 6, 8, 10 wt%) were coded as PU/AChN-2, PU/AChN-4, PU/AChN-6, PU/AChN-8 and PU/AChN-10. Meanwhile, neat PU film was prepared and coded as PU according to the aforementioned process without the addition of

AChN. All the films were vacuum-dried at room temperature for 3 days before the measurements.

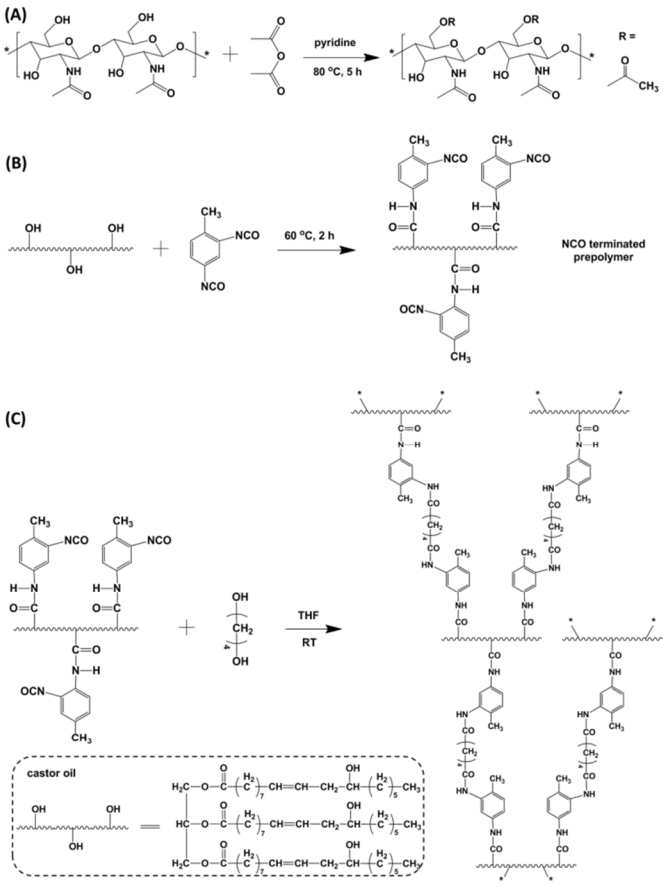

Figure 1. (A) Partial surface acetylation of chitin nanocrystals from chemcial reaction between hydroxyl groups (C6-OH) and acetic anhydride. (B) Chemical structure of NCO terminated polyurethane prepolymers. (C) Synthesis procedure of polyurethane materials and chemical structures of castor oil.

Analysis and Characterization.

Elemental Analysis. Contents of carbon (C%), nitrogen (N%) and hydrogen (H%) were obtained from elemental analysis (Elementar Vario EL cube, Germany). The precision of measurements is 0.01% for C and N, and 0.001% for H. Degree of acetylated substitution ($DS_{\text{surface acetyl}}$) for AChN was calculated according to eqn (1):

$$DS_{surface\ acetyl} = \frac{n_{surface\ acetyl}}{n_{surface-OH}} = \frac{[\Delta C\%/12]/2}{n_{surface-OH}} \quad (1)$$

where $n_{\text{surface acetyl}}$ is the amount of surface acetyl groups on AChN (without considering acetyl group on C-2 itself), $n_{\text{surface-OH}}$ is the amount of surface hydroxyl groups on nanocrystals, and $\Delta C\%$ is the increment of carbon content after surface acetylation ($\Delta C\% = C\%_{\text{AChN}} - C\%_{\text{ChN}}$).

Morphology and Dimensions. The morphology of acetylated chitin nanocrystals was observed with transmission electron microscopy (TEM), which was carried out on an H-7000FA electron microscope (Hitachi, Tokyo, Japan) at 75 kV. Aqueous suspension (about 0.1 wt%) containing AChN was homogeneously dispersed with ultrasonic treatment, and then negatively stained with a 2% (w/v) uranyl acetate in ethanol solution before the observation. The dimensions of AChN, including length (L) and width (W) of nanoparticles, were measured by the software of Nano Measurer. Over 100 rod-like nanocrystals from 10 TEM images were statistically analyzed to determine the average length, width, and distribution.

Crystalline Property. The transformation of crystalline structure for chitin nanocrystals before and after modification as well as the crystalline property of nanocomposites were analyzed using X-ray diffraction analysis (XRD). XRD measurements were performed on a D/Max-IIIA X-ray diffractometer (Rigaku Denki, Tokyo, Japan) at ambient temperature, with Cu Ka radiation (λ=0.154 nm) at 40 kV and 60 mA. The diffraction angle of 2θ ranged from 5 to 50°.

The crystallinity index ($CrI_{2\theta}$) of ChN and AChN were calculated according to Segal equation:

$$CrI_{2\theta} = \frac{I_{2\theta} - I_{am}}{I_{2\theta}} \times 100\% \quad (2)$$

In eqn (2), $I_{2\theta}$ is the overall intensity of the peak at 2θ, and I_{am} represents the intensity of amorphous diffraction at 16.0°.

Crystalline dimensions of different planes of nanocrystals were calculated according to Scherrer equation:

$$B_{hkl} = \frac{K\lambda}{\beta_{1/2} cos\theta} \quad (3)$$

In eqn (3), B_{hkl} is the average crystalline width of a specific plane; K is a constant (indicative of crystallite perfection and was assumed to be 0.9; λ represents the wavelength of incident X-rays (λ = 0.15418 nm); θ is the center of the peak; and $\beta_{1/2}$ (in radius) represents the full width at half maximum (FWHM) of the reflection peak.

Simultaneous Thermal Analysis (STA: TG/DSC). STA technique is useful for the determination of decomposition temperatures and steps for solid samples, which involving simultaneous thermogravimetric analysis and differential scanning calorimetry analysis. The thermal degradation of native chitin, ChN and AChN were analyzed by a thermal analyzer STA 449G Jupiter (Nietzsch, Germany) under air flow. Samples of ca. 10 mg were heated from 20 to 600 °C at a heating rate of 10 °C/min.

Atomic Force Microscopy (AFM). Surface morphology of PU/AChN nanocomposites was investigated by AFM under QNM mode analysis. The film sample was placed on the surface of steel substrate, which was scanned at a frequency < 1 Hz, and changing the rate according to the scan size.

Transmittance of Visible Light. Light transmittance ratios of nanocomposites were measured with a Shimadzu UV 2401-(PC) UV−vis spectrophotometer. The film samples were cut at 40 mm × 35 mm, and analyzed within a wavelength range of 200–800 nm. The transmittance spectra were acquired using air as background. The resolution of the spectrophotometer was 1.5 nm and the photometric accuracy was ±0.01 in absorption.

Tensile Measurements. The tensile strength (σ_b), elongation at break (ε_b) and Young's modulus (E) were measured on a CMT6503 universal testing machine (SANS, Shenzhen, China) with a crosshead rate of 10 mm/min according to the protocol of ISO 527-3:1995(E). The tested specimens were cut into quadrate strips with the width of 10 mm, and the distance between testing marks was 30 mm. The average value of at least five replicates of each sample was taken.

Differential Scanning Calorimetry (DSC). The thermal property of PU/AChN nanocomposites was characterized by DSC analysis on a DSC-instrument (Diamond DSC, PerkinElmer, MA) under a

nitrogen atmosphere at a heating or cooling rate of 20 °C/min. The nanocomposite samples were scanned over a range of –50 to 200 °C after a pretreatment of heating from 20 to 100 °C and then cooling to –50 °C to remove the residual solvent or other volatile.

Fourier Transform Infrared Spectroscopy (FTIR). The interactions of hydrogen bondings in PU/AChN nanocomposites were investigated by FTIR spectra, which were recorded on a 5700 FTIR spectrometer (Thermo Fisher, Madison, WI). The samples of nanocomposites were scanned in the range of 4000–600 cm^{-1}.

Scanning Electron Microscope (SEM). Microstructure of PU/AChN nanocomposites were observed on SEM, which were carried out on a X-650 scanning electron microscope (Hitachi, Tokyo, Japan) with an accelerating voltage of 25 kV. Before the observation, all films were frozen in liquid nitrogen and then immediately snapped. The fracture surfaces of the sheets were sputtered with gold and then observed and photographed.

Results and discussion

Acetylation and Properties of Chitin Nanocrystals

The feasibility of surface acetylation on chitin nanocrystals with acetic anhydride has been validated by the results of solid state ^{13}C cross polarization-magic angle spinning (CP-MAS) NMR spectra and FT-IR in our previous study.[27] In here, the DS value of surface acetyl groups to surface hydroxyl groups ($n_{surface\text{-}OH}$) was calculated from the change of carbon contents in nanocrystals before and after modification. Table 1 summarized the results from elemental analysis and estimated $DS_{surface\ acetyl}$ value according to eqn (1). In general, because the acetylation was controlled on the surface of chitin nanocrystals, the change of elemental contents was slight. However, the carbon content of acetylated chitin nanocrystals (AChN) significantly increased due to the replacement of hydroxyl groups to acetyl groups on nanocrystals. The change of C/N ratios for nanocrystals before and after modification further proved the presence of acetylation on the surface of nanoparticles. Before the estimation of surface acetyl degree of substitution ($DS_{surface\ acetyl}$) for AChN, the total amount of surface active hydroxyl groups ($n_{surface\text{-}OH}$) on chitin nanocrystals was calculated from theoretical models of nanocrystals,[28] which was about 1.55 mmol/g (detailed calculation was shown in Supplemental Information). Then, the $DS_{surface\ acetyl}$ of AChN (corresponding to surface hydroxyl groups) was estimated as 51.1% according to eqn (1), which indicated about half of surface hydroxyl groups was substituted by acetyl groups during the modification. Due to the different reactivity of two hydroxyl groups on the structure of chitin (generally accepted as C6-OH > C3-OH), this result reflected the substitution of one hydroxyl groups (C6-OH), and meanwhile the preservation of another hydroxyl groups (C3-OH). Consequently, using the reactive condition in this study (reagents ratio of 1.0 g ChN/5 mL AA, reaction duration of 5 h), partial surface acetylation on chitin nanocrystals can be achieved, and original crystalline structure of nanocrystals can also preserved (as discussed in following results). In fact, different reactive ratios and duration of acetylation were also attempted on chitin nanocrystals in our experiments (with the range of 1.0 g ChN/2-10 mL AA for 2-12 h), which proved the controllability of varied $DS_{surface\ acetyl}$ for chitin nanocrystals by changing the reactive conditions of this method.

As same as cellulose nanocrystals, the main challenge towards chemical modification of chitin nanocrystals is to conduct a reaction taking place on the surface of nanoparticles, while preserving the original morphology and structure to avoid any polymorphic conversion for crystalline integrity.[29] As shown in TEM images in Figure 2, after the surface acetylation, AChN maintained the rod-like morphology and exhibited better dispersion in comparison with pristine ChN (reported in our previous studies).[27] Further statistical analysis of dimensions (length and diameter) and distribution of AChN was made by Nanoscope software (Figure S1 in Supporing Information). With the measurement of over 100 individual nanocrystals from TEM images (mainly focusing on the images with the enlargement of × 25000), the average length and diameter of AChN were about 211.6 nm and 12.2 nm, which were similar as the dimensions of pristine ChN (as shown in Table 1).

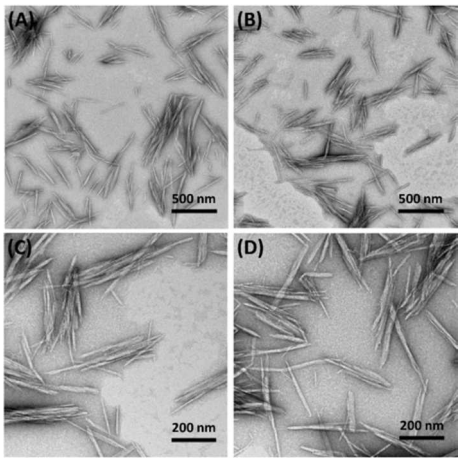

Figure 2. TEM images of acetylated chitin nanocrystals (AChN) at different observation scales. (A and B) × 9600; (C and D) × 25000

Crystalline property is one of the most important physical properties of chitin nanocrystals, which reflects the integrity of original structure of nanocrystals after surface modification. The X-ray diffraction patterns of ChN and AChN were shown in Figure 3, and the values of crystallinity index (CrI, %) and crystalline dimensions

Table 1. Dimensions (average length *L* and diameter *D*) of ChN and AChN were obtained from TEM images; carbon (C%), nitrogen (N%) and hydrogen (H%) contents for chitin nanocrystals before and after acetylation (ChN and AChN) were measured by elemental analysis; amount of surface hydroxyl groups ($n_{surface\text{-}OH}$) of chitin nanocrystals was calculated with theoretical models (Supporting Information); and surface acetyl degree of substitution ($DS_{surface\ acetyl}$) for AChN was calculated according to eqn (1).

Samples	Length	Diameter	C	N	H	C/N	$n_{surface\text{-}OH}$	$DS_{surface\ acetyl}$
	nm	nm	%	%	%		mmol/g	%
ChN	217.0±72.1	12.4±3.7	43.56	6.38	6.323	7.96	1.55	—
AChN	211.6±67.4	12.2±3.4	45.46	6.15	6.356	8.62	—	51.1

in different planes were summarized in Table 2. The characteristic diffraction peaks of crystallite crab chitin were observed on the patterns of both ChN and AChN, located at 2θ angles of around 9.3°, 19.2°, 20.7°, 23.4°, and 26.3° corresponding to typical reflection planes of α-chitin, 020, 110, 120, 101, and 130 respectively. The crystallinity index of chitin nanocrystals were calculated from two peaks CrI_{020} and CrI_{110} according to the Segal method.[30,31] In general, the high crystallinity index (about 80%) of both ChN and AChN proved the maintenance of crystalline integrality for nanocrystals during the surface acetylation. In addition, the crystalline dimensions of different planes (B_{020} and B_{110}) of nanocrystals can be calculated according to the Scherrer equation. As shown in Table 2, the result of no change and only slight decrease of crystalline sizes in 110 and 020 planes indicated the preservation of crystalline structure for chitin crystallites during the modification.[32]

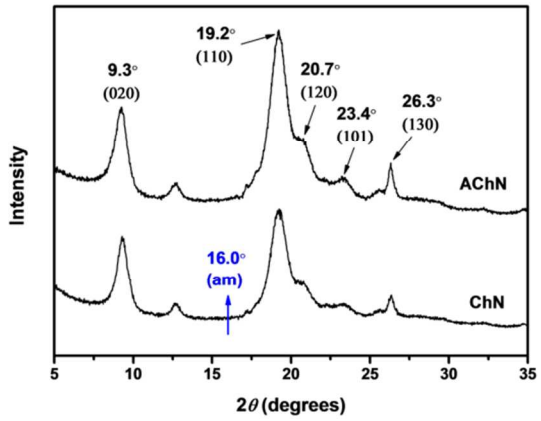

Figure 3. X-ray diffraction patterns of ChN and AChN samples.

Table 2. Values of crystallinity index (CrI_{020}, CrI_{110}) and crystalline dimensions (B_{020}, B_{110} and B_{130}) of chitin nanocrystals before and after acetylation.

Samples	Crystalline index		Crystalline dimensions	
	CrI_{020} (%)	CrI_{110} (%)	B_{020} (nm)	B_{110} (nm)
ChN	78.2	83.0	9.9 ± 0.06	6.7 ± 0.02
AChN	73.6	84.0	8.7 ± 0.04	6.4 ± 0.02

Due to the use of tetrahydrofuran (THF) as the solvent for the system of polyurethane-based materials, the dispersion of AChN in THF will affect its reinforcing effect in nanocomposites. Pristine ChN tended to self-aggregation in organic solvents attributed to the strong interactions from rich hydrophilic hydroxyl groups on the surface of nanoparticles. As shown in Figure 4, pristine ChN quickly sedimented to the bottom of THF suspension after the standing of 30 min. However, the THF suspension containing AChN showed outstanding dispersion and stability during the 12 h standing, which indicated the significant improvement of dispersibility of chitin nanocrystals after surface acetylation. The good dispersion of AChN in THF derived from the replacement of hydrophilic hydroxyl groups to hydrophobic acetyl groups, and the weakening of intra- and intermolecular hydrogen bonding among nanoparticles.

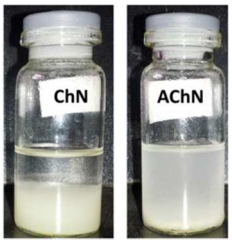

Figure 4. The dispersibility observation of ChN (with the standing of 30 min in 4 °C) and AChN (with the standing of 12 h in 4 °C) in the solvent of tetrahydrofuran.

The influence of surface acetylation to thermal stability of chitin nanocrystals was investigated by simultaneous thermal analysis (TG/DSC), as shown in Figure 5. From TG curves, the thermal degradation of native chitin appeared at about 270 °C, while pristine ChN started to degrade at about 200 °C. Interestingly, after surface acetylation, the degradation temperature of AChN was about 65 °C higher than that of pristine ChN, which indicated the enhancement of thermal stability of nanocrystals from the presence of stable acetyl groups. In addition, a wide endothermic peak coupled with weight-loss appeared on DSC curves for ChN or AChN when heated between 350 and 450 °C, which was primarily attributed to the depolymerization of chitin with the formation of volatile low molecular products and char.[33]

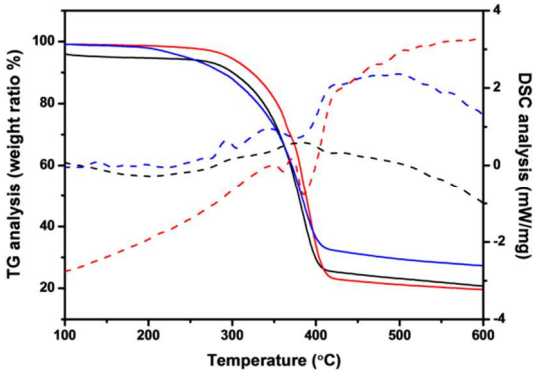

Figure 5. TG and DSC curves of native crab chitin (black curves), ChN (blue curves) and AChN (red curves) obtained from simultaneous thermal analysis at a heating rate of 10 °C/min. Solid curves (TG analysis), dash curves (DSC analysis).

Appearance and light transmittance ratio of nanocomposites

As mentioned before, rigid chitin nanocrystals with high specific modulus was a promising candidate as nano-reinforcing biofiller in composites. Furthermore, different from the micro-sized fillers, the introduction of chitin nanocrystals will not sharply affect the optical transparence of composites even with the high filler concentrations.[34] Figure 6(A) showed the pictures of PU-based nanocomposites containing different contents of AChN. In general, all nanocomposites exhibited the (semi-)transparent appearance similar as neat castor oil-based PU material, because the well-dispersed and individual AChN with 10–20 nm width was sufficiently thinner than the wavelength of visible light from approximately 400 nm to 700 nm.[35] Polyurethane is a kind of thermoplastic and "soft" polymer with special high-elasticity property. Interestingly, this mechanical property was also kept in AChN-loaded composites in spite of the presence of rigid AChN nanoparticles in soft PU

matrix (taken PU/AChN-6 sample as the example in Figure 6B).

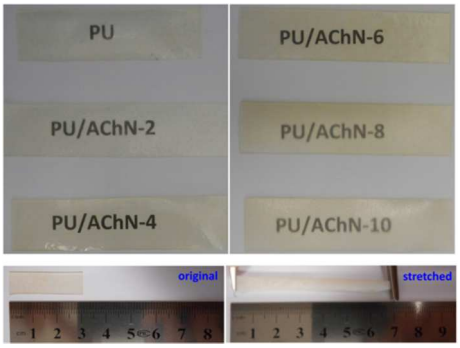

Figure 6. (A) Pictures of thermoplastic PU-based nanocomposites filled with various contents of AChN. (B) Simple stretching test to check the preservation of high-elasticity of PU-based nanocomposites (sample PU/AChN-6).

The light transmittance ratio of nanocomposites was further measured by UV spectrophotometer, as shown in Figure 7. The result of high transmittance ratio for all composites (> 40% under the visible light of 700 nm) indicated the slight influence of AChN in PU matrix. Specifically, in comparison with neat PU material, composites PU/AChN-2 and PU/AChN-4 showed a little increase of light transmittance ratio, which can be attributed to the homogeneous dispersion and nano-sized effect of AChN in composites. However, high loading levels of AChN in composites may cause the aggregation of nanoparticles, which will induce the transformation of individual nanofillers to larger nanophases, and therefore result in the gradual reduction of transmittance ratio of composites (particularly samples PU/AChN-8 and PU/AChN-10).

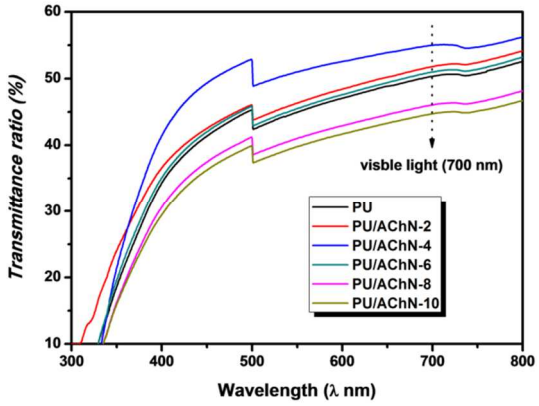

Figure 7. UV transmittance spectra of AChN-filled PU nanocomposites.

It was reported that nanochitin (chitin nanocrystals and chitin nanofibers) possessed appropriate filtering speed (9 times faster than nanocellulose),[36] which was favorable to the evaporation of moisture and formation of smooth films from suspensions. The surface morphology of nanocomposites was observed by AFM using QNM and Tapping modes. As shown in Figure 8, the composite PU/AChN-2 (image B) containing low content of nanofillers exhibited the flat surface similar as neat PU material (image A). The slight asperity of the appearance on two images may result from the bubbles during casting-evaporation treatment. In comparison with neat PU, uniform and regular aspect was observed on the amplitude and height images of the composite PU/AChN-6 (images C and D), which indicated good compatibility and miscibility of AChN nanoparticles in polymeric matrix. Regarding the composites PU/AChN-2 and PU/AChN-6, it was difficult to catch the "face" of AChN on the surface images, which may be attributed to the dispersion and existence of nanoparticles inside the composites under these concentrations. However, when checking the surface of the composite PU/AChN-10, nanoscaled dots in some regions were observed from the height image (image E), which reflected the presence of some AChN nanoparticles on the surface of this composite. Interestingly, due to the presence of AChN in different orientation, varied shapes and morphologies of these dots from the PU/AChN-10 composite were caught by further enlargement of images. As shown in the phase image (F), white parts in the shapes of cylinder, dot and irregularity may correspond to the lying, vertical end and aggregation of AChN nanoparticles.

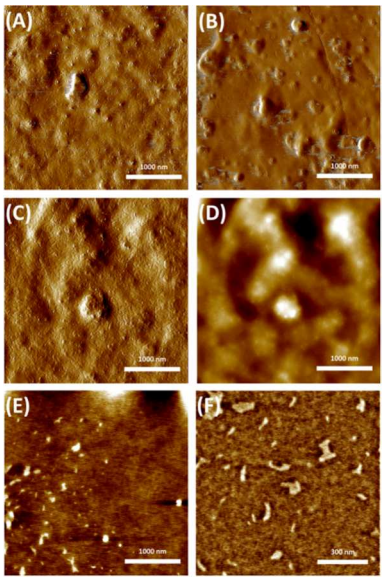

Figure 8. AFM images of surface morphology of nanocomposites: (A) amplitude image of PU, (B) amplitude image of PU/AChN-2, (C) amplitude image of PU/AChN-6, (D) height image of PU/AChN-6, (E) height image of PU/AChN-10, (F) phase image of PU/AChN-10.

Mechanical and Thermal Properties of Nanocomposites

Improvement of mechanical properties (particularly stiffness) upon adding pristine chitin nanocrystals was observed for almost all polymeric matrices in pioneering studies.[37,38] The interaction between nanoparticles to form the percolating network was proposed to explain the nano-reinforcement of rigid chitin nanocrystals in composites. In order to further enhance the interfacial adhesion between chitin nanocrystals and polymeric matrices, chemical modification was attempted to perform on chitin nanocrystals, such as surface derivatization with phenyl isocyanate, alkenyl succinic, or 3-isopropenyl-α,α′-dimethylbenzyl isocyanate.[14] However, the introduction of these modified chitin nanocrystals in natural rubber induced the loss of mechanical properties of ensuing composites, which was ascribed to the limited hydrogen bonding interactions between nanocrystals after the replacement of surface hydroxyl groups and the reduction of driving force for network formation. In this study, partial acetylation of chitin nanocrystals (substitution of C6-OH) was expected to improve the interfacial compatibility between modified nanocrystals and PU matrix; meanwhile surface

hydroxyl groups (C3-OH) was preserved for the formation of rigid network among nanocrystals in composites. Figure 9 showed the effects of various AChN contents on the mechanical properties of PU-based compostes, involving tensile strength (σ_b), Young's modulus (E) and elongation at break (ε_b). Attributed to the presence of rigid AChN, Young's modulus of nanocomposites gradually enhanced with the increase of nanocrystal contents, particularly from 0.98 MPa for neat PU material to 1.87 MPa and 4.01 MPa for composites PU/AChN-6 and PU/AChN-10. On the other hand, nano-reinforcing effect of AChN promoted the increase of tensile strength of nanocomposites, such as highest value of 5.67 MPa for PU/AChN-6 in comparison with only 2.79 MPa for neat PU material. Regarding the breaking elongation of nanocomposites, there was an increase for composites PU/AChN-2 and PU/AChN-4, and then the reduction tendency for the composites with AChN loading levels of higher than 6 wt% in comparison with neat PU material.

As mentioned before, through the strong hydrogen bonding among nanoparticles (from retained C2-OH on the surface of AChN), the rigid percolating network can form, and contribute the improvement of mechanical properties for nanocomposites. The percolating threshold value is determined by the aspect ratio (L/D) of rod-like nanoparticles, and can be calculated according eqn (4):[39]

$$\omega_{Rc} = \frac{0.7}{L/D} \times \rho_{chitin} \times 100\% \quad (4)$$

In this study, the aspect ratio of AChN was estimated as 17.4 from the results of Table 1, so the calculated value of ω_{Rc} was about 5.7 wt% for PU/AChN composites. Under low contents of nanofillers, mechanical properties of composites were dependent on interfacial interactions between nanofillers (AChN) and matrix (PU), which showed slight increase of tensile strength and breaking elongation for PU/AChN-2 and PU/AChN-4. Three-dimensional network from AChN can form in composites with AChN loading levels higher than percolating threshold, such as PU/AChN-6 and PU/AChN-8. Attributed to the presence of rigid network and stress transferring, both Young's modulus and tensile strength of the composite PU/AChN-6 was advanced about 2 times in comparison with neat PU material. However, superfluous nanofillers will induce the self-aggregation of AChN and further microstructure separation, which may result in the reduction of strength and tenacity of the composite (PU/AChN-10), despite the sharp increase of modulus (from rigid network).

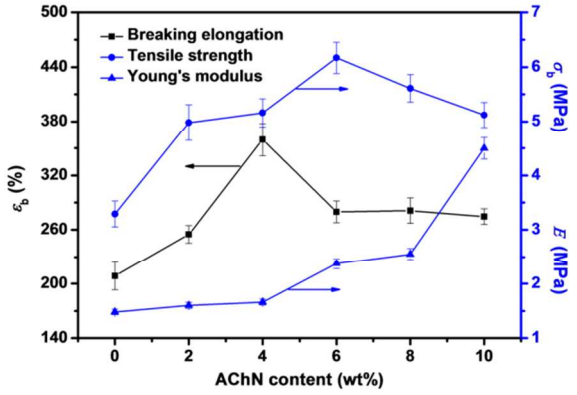

Figure 9. Mechanical performance and nano-reinforcing effect of various loading levels of AChN on tensile strength (σ_b), Young's modulus (E) and elongation at break (ε_b) of PU-based composites.

Thermal properties of materials are of importance for processing issues and the practical application. Regarding thermoplastic polyurethane-based materials, the glass transition temperature (T_g) is special significant characteristics since this value can affect the performance of materials, including mechanical behavior, swelling property etc. The glass transition temperature is a parameter at which a polymer changes from hard and brittle (glassy state) to soft and ductile (rubbery state). DSC is the most common technique to measure the T_g of materials. Original DSC thermograms of PU/AChN nanocomposites were shown in Figure S2 (Supporting Information), and some data on glass transition of nanocomposites were summarized in Table 3. On the whole, it was observed that the T_g values of nanocomposites gradually increased with the increase of AChN contents. Two factors from the addition of reinforcing nanophase in composites can be used to explain this phenomenon. The presence of rigid nanoparticles (AChN) and possible rigid network will restrict the free mobility of soft segments of PU polymers. Moreover, because of the surface acetylation, co-crystallization may occur between PU chains and neighboring nanocrystals, which will enhance the interactions between soft and hard segments of polymeric matrix. Similar result of T_g increase with the introduction of rigid nanoparticles was also reported by the system of water polyurethane/cellulose nanocrystals.[40]

Table 3. Heat-capacity increment during the glass transition (ΔC_p), glass transition temperatures measured as the onset ($T_{g,\ onset}$), midpoint ($T_{g,\ mid}$), and endpoint ($T_{g,\ end}$) temperature of PU/AChN nanocomposites from DSC thermograms.

Samples	ΔC_p (J/g·°C)	$T_{g,\ onset}$ (°C)	$T_{g,\ mid}$ (°C)	$T_{g,\ end}$ (°C)
PU	0.226	−1.44	5.90	13.21
PU/AChN-2	0.238	−0.37	5.86	12.51
PU/AChN-4	0.279	0.80	7.25	13.93
PU/AChN-6	0.213	1.79	6.52	12.07
PU/AChN-8	0.254	1.27	7.22	13.55
PU/AChN-10	0.432	4.11	8.40	12.68

Crystalline Property and Microstructure of Nanocomposites

The X-ray diffraction (XRD) of neat PU material and PU/AChN composites containing different contents of AChN were presented in Figure 10. A wide diffused diffraction peak located at 2θ of about 19°–20° appeared on all XRD patterns of polyurethane-based materials, which was assigned to a short-range-order arrangement of chain segments of polyurethane molecules.[41] Regarding the composites loaded with low contents of AChN (≤ 6 wt%), no obvious diffraction peak of chitin was observed, which indicated the well-dispersed nanocrystals without any large agglomeration in these composites. However, a weak diffraction peak at 2θ of 19.2° was visible on the pattern of the composite PU/AChN-10, which can be identified as the characteristic peak corresponding to the 110 reflection of chitin. The presence of crystalline feature of chitin nanocrystals reflected the preservation of original structure of nanocrystals in composites, but slight aggregation of nanoparticles in the composite PU/AChN-10.

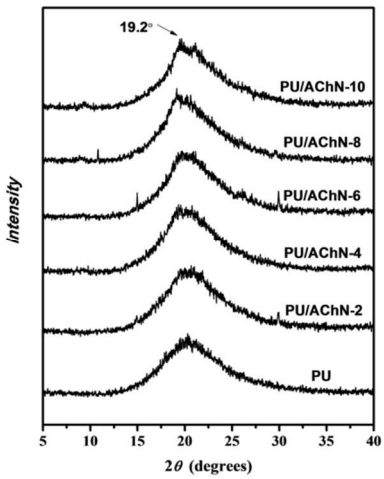

Figure 10. XRD patterns of PU/AChN nanocomposites and neat PU material.

The hydrogen bonding in polyurethane-based materials can be investigated by Fourier transform infrared spectroscopy (FTIR) spectra, as shown in Figure 11. Two important stretching regions for polyurethane, located at 3600–3100 cm^{-1} and 1800–1650 cm^{-1}, were observed to analyze the effect of rigid AChN on the hydrogen bonding and phase separation of segmented PU-based composites. It was reported that in polyurethane, the infrared peaks at 3480 and 3320 cm^{-1} were assigned to the free N–H stretching and the hydrogen-bonded N–H stretching, while the bands at 1733 and 1703 cm^{-1} were associated with the free-of-hydrogen-bonding C=O stretching and the hydrogen-bonded C=O stretching.[42] On the chemical structure of acetylated chitin nanocrystal, additional acetyl groups (with carbonyl) allowed for increased hydrogen bonding between nanocrystals and adjacent polymer chains. Indeed, the hydrogen atoms of N–H groups from the hard segment of polyurethane component can serve as proton donors, and the acetyl carbonyl groups of AChN as well as the urethane carbonyl groups were expected as proton acceptors.[2] As shown in Figure S3 (Supporting Information), strong hydrogen-bonded N–H stretching peaks appeared on the spectra of all composites, while weak or even no signal was observed for free N–H stretching.[43] This result indicated the high degree of hydrogen-bonded N–H groups in composites after the addition of AChN nanoparticles. On the other hand, regarding the C=O stretching located at 1733 and 1703 cm^{-1} (Figure S3 in Supporting Information), the intensities of hydrogen-bonded C=O stretching peaks slightly increased with the higher loading levels of AChN in composites. From the result of FTIR, higher degree of hydrogen-bonded than free N–H or C=O stretching may reflected the good compatibility and enhanced interfacial interactions between acetylated chitin nanocrystals and polyurethane in composites.

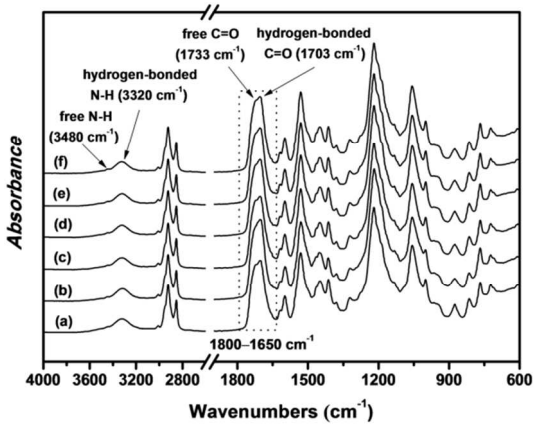

Figure 11. FTIR spectra of PU/AChN nanocomposites and neat PU material. (a) PU, (b) PU/AChN-2, (c) PU/AChN-4, (d) PU/AChN-6, (e) PU/AChN-8, (f) PU/AChN-10.

The microstructure of PU/AChN nanocomposites was further observed from the fracture morphology by scanning electron microscope (SEM). As shown in Figure 12, derived from the homogeneous dispersion, the presence of low-loading levels of AChN showed rare influence to the structure of PU-based composites (PU/AChN-2 and PU/AChN-4), which provided the flat and uniform fractured morphologies (images B and C) similar as neat PU material (image A). The composite PU/AChN-6 (image D) exhibited the slightly coarse and irregular fractured morphologies, which indicated some changes of the composite microstructure. As mentioned before, rigid percolating network can form in composites under this loading level of AChN, which will restrict the free mobility of soft segments of polyurethane polymers. Higher contents of AChN caused the coarser fractured morphologies of composites, such as PU/AChN-8 (image E) and PU/AChN-10 (image F). Particularly regarding the composite PU/AChN-10, inhomogeneity and microphase separation between reinforcing nanophases and polymeric matrix may exist to some extent, because of the addition of superfluous AChN nanoparticles.

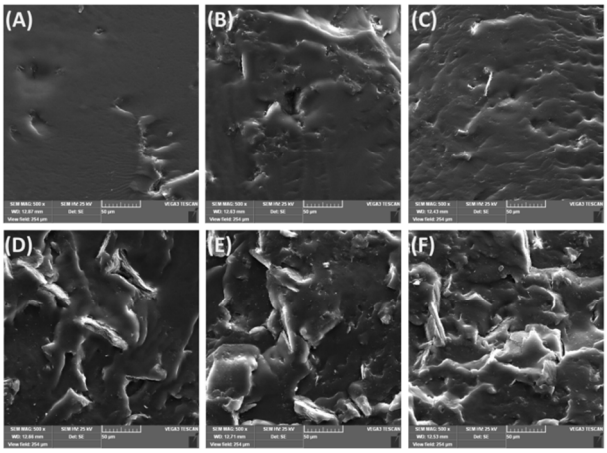

Figure 12. Fracture morphology of PU/AChN nanocomposites with various AChN contents. (A) PU, (B) PU/AChN-2, (C) PU/AChN-4, (D) PU/AChN-6, (E) PU/AChN-8, (F) PU/AChN-10.

Conclusions

In conclusion, novel elastomeric nanocomposites were developed with high-crystallinity "rigid" chitin nanocrystals as biobased fillers and high-elasticity "soft" polyurethane as polymeric matrix. Through the treatment of controlled surface acetylation, hydrophilic hydroxyl groups (C6-OH) on the surface of chitin nanocrystals were partially converted as hydrophobic acetyl groups, which was favorable to the improvement of compatibility and hydrogen bonding interactions between nanofillers and matrix. Furthermore, from other preserved hydroxyl groups (C3-OH), rigid three-dimensional network among acetylated chitin nanocrystals can form under the critical concentration in composites, which provided the enhancement of stiffness and toughness of thermoplastic polyurethane-based nanocomposites. With the addition of 6 wt% acetylated chitin nanocrystals, the castor oil-based nanocomposite with tensile strength of 5.67 MPa, elongation at break of 280.0% and Young's modulus of 1.87 MPa was obtained, which were surpassed those of 103%, 40% and 91% in comparison with neat polyurethane material. In this study, the proposed strategy of "tradeoff" between interfacial adhesions from nanofillers and matrix and formation of network from nanofillers provided an approach to incorporate rigid nanofillers to polymeric matrices and elastomers. The discussion and results of this study are expected to enrich the nano-reinforcing mechanism of biobased chitin nanocrystals in composite materials, and further broaden the practical use of natural polymers as novel high-added products.
The conclusions section should come at the end of article, before the acknowledgements.

Acknowledgements

The authors thanks to the support of National Natural Science Foundation of China (51373131), Project of New Century Excellent Talents of Ministry of Education of China (NCET-11-0686), and Fundamental Research Funds for the Central Universities (Self-Determined and Innovative Research Funds of WUT).

Notes and references

[a] Department of Chemical Engineering, College of Chemistry, Chemical Engineering and Life Sciences, Wuhan University of Technology, Wuhan 430070, China.

[b] Grenoble Institute of Technology (Grenoble INP) – The International School of Paper, Print Media and Biomaterials (Pagora), CS10065, 38402 Saint Martin d'Hères Cedex, France.

[c] College of Materials Science and Engineering, Wuhan University of Technology, Wuhan 430070, China.

† Electronic Supplementary Information (ESI) available: Models and formulas for the calculation of amount of surface hydroxyl groups ($n_{surface-OH}$) on chitin nanocrystals, size statistics for the length (L) and diameter (D) of acetylated chitin nanocrystals, original DSC thermograms and amplified FTIR spectra at the regions of 3600–3100 cm^{-1} and 1800–1650 cm-1 of PU/AChN nanocomposites were shown in Supporting Information. See DOI: 10.1039/b000000x/

To whom correspondence should be addressed.
* Corresponding Author: Jin Huang, Email: huangjin@iccas.ac.cn
Phone/Fax: 86-27-87749379

1 A. Okada, Y. Fukoshima, S. Inagaki, A. Usuki, S. Sugiyama, T. Kurauchi and O. Kamigaito, *US Patent* 1988, 4.739.007.
2 A. Pei, J.-M. Malho, J. Ruokolainen, Q. Zhou and L.A. Berglund, *Macromolecules* 2011, **44**, 4422.
3 S. Thomas, and R. Stephen, Rubber nanocomposites: preparation, properties and applications. John Wiley & Sons (Asia) Pte Ltd, Singapore, 2010, pp. 705.
4 A. Dufresne, S. Thomas and L.A. Pothan, Biopolymer nanocomposites: processing, properties, and applications. John Wiley & Sons Inc., Hoboken, New Jersey, 2013, pp. 696.
5 R.H. Marchessault, F.F. Morehead and N.M. Walter, *Nature* 1959, **184**, 632.
6 J.F.V. Vincent and U.G.K. Wegst, *Arthropod Struct. Dev.* 2004, **33**, 187.
7 J.-B. Zeng, Y.-S. He, S.-L. Li and Y.-Z. Wang, *Biomacromolecules* 2012, **13**, 1.
8 M. Mincea, A. Negrulescu and V. Ostafe, *Rev. Adv. Mater. Sci.* 2012, **30**, 225.
9 K.G. Nair and A. Dufresne, *Biomacromolecules* 2003, **4**, 657.
10 K.G. Nair and A. Dufresne, *Biomacromolecules* 2003, **4**, 666.
11 A. Saralegi, S.C.M. Fernandes, A. Alonso-Varona, T. Palomares, E.J. Foster, C. Weder, A. Eceiza, M.A. Corcuera, *Biomacromolecules* 2013, **14**, 4475.
12 J. Huang, J.W. Zou, P.R. Chang, J.H. Yu and A. Dufresne, *Express Polym. Lett.* 2011, **5**, 362.
13 M. Zeng, H. Gao, Y. Wu, L. Fan and A. Li, *J. Macromol. Sci. A* 2010, **47**, 867.
14 K.G. Nair and A. Dufresne, *Biomacromolecules* 2003, **4**, 1835.
15 S. Ifuku, S. Morooka, M. Morimoto and H. Saimoto, *Biomacromolecules* 2010, **11**, 1326.
16 N. Lin, J. Huang, P.R. Chang, J. Feng and J. Yu, *Carbohydr. Polym.* 2011, **83**, 1834.
17 S. Lin, J. Huang, P.R. Chang, S. Wei, Y. Xu and Q. Zhang, *Carbohydr. Polym.* 2013, **95**, 91.
18 D.S. Ogunniyi, *Bioresource Technol.* 2006, **97**, 1086.
19 H. Mutlu and M.A.R. Meier, *Eur. J. Lipid Sci. Technol.* 2010, **112**, 10.
20 E. Hablot, D. Zheng, M. Bouquey and L. Avérous, *Macromol. Mater. Eng.* 2008, **293**, 922.
21 M.A. Corcuera, L. Rueda, B. Fernandez d'Arlas, A. Arbelaiz, C. Marieta, I. Mondragon and A. Eceiza, *Polym. Degrad. Stabil.* 2010, **95**, 2175.
22 K.M.S. Meera, R.M. Sankar, J. Paul, S.N. Jaisankar and A.B. Mandal, *Phys. Chem. Chem. Phys.* 2014, **16**, 9276.
23 A. Saralegi, M.L. Gonzalez, A. Valea, A. Eceiza and M.A. Corcuera, *Compos. Sci. Technol.* 2014, **92**, 27.
24 S.A. Madbouly, Y. Xia and M.R. Kessler, *Macromolecules* 2013, **46**, 4606.
25 N. Lin, J. Huang, P.R. Chang, L. Feng and J. Yu, *Colloid. Surface. B* 2011, **85**, 270.
26 S. Gao and L. Zhang, *Macromolecules* 2001, **34**, 2202.
27 Q. Zhang, S. Wei, J. Huang, J. Feng and P.R. Chang, *J. Appl. Polym. Sci.* 2014, **131**, 39809.
28 N. Lin, J. Huang and A. Dufresne, *Nanoscale* 2012, **4**, 3274.
29 N. Lin, and A. Dufresne, *Nanoscale* 2014, **6**, 5384.
30 L. Segal, J.J. Creely, A.E. Martin and C.M. Conrad, *Text. Res. J.* 1959, **29**, 786.
31 Y. Zhang, C. Xue, Y. Xue, R. Gao and X. Zhang, *Carbohydr. Res.* 2005, **340**, 1914.

32 Y. Wang, Y. Chang, L. Yu, C. Zhang, X. Xu, Y. Xue, Z. Li and C. Xue, *Carbohydr. Polym.* 2013, **92**, 90.
33 W. Tang, C. Wang and D. Chen, *Polym. Degrad. Stabil.* 2005, **87**, 389.
34 S. Ifuku and H. Saimoto, *Nanoscale* 2012, **4**, 3308.
35 M. Nogi, K. Handa, A.N. Nakagaito and H. Yano, *Appl. Phys. Lett.* 2005, **87**, 243110.
36 M.I. Shams, S. Ifuku, M. Nogi, T. Oku and H. Yano, *Appl. Phys. A.* 2011, **102**, 325.
37 M. Paillet and A. Dufresne, *Macromolecules* 2001, **34**, 6527.
38 A. Morin and A. Dufresne, *Macromolecules* 2002, **35**, 2190.
39 A. Dufresne, Nanocellulose: from nature to high performance tailored materials. Walter de Gruyter GmbH, Berlin and Boston, MA, 2012, pp. 460.
40 X. Cao, Y. Habibi and L.A. Lucia, *J. Mater. Chem.* 2009, **19**, 7137–7145.
41 Y.I. Tien and K.H. Wei, *Polymer* 2001, **42**, 3213.
42 R.W. Seymour, G.M. Estes and S.L. Cooper, *Macromolecules* 1970, **3**, 579.
43 X. Yao, X. Qi, Y. He, D. Tan, F. Chen and Q. Fu, *ACS Appl. Mater. Interfaces* 2014, **6**, 2497.

